JOURNAL OF GEOPHYSICAL RESEARCH, VOL. 114, D04102, doi:10.1029/2008JD010519, 2009

Regional cooling in a warming world: Recent temperature trends in the southeast Pacific and along the west coast of subtropical South America (1979–2006)

Mark Falvey[1] and René D. Garreaud[1]

Received 30 May 2008; revised 13 November 2008; accepted 9 December 2008; published 18 February 2009.

[1] While it is widely accepted that the global mean atmospheric temperature has increased in recent decades, the spatial distribution of global warming has been complex. In this study we comprehensively characterize the spatial pattern, including vertical structure, of temperature trends along the subtropical west coast of South America (continental Chile) for the period 1979–2006 and examine their consistency with expectations based on the CMIP-3 ensemble of coupled ocean-atmosphere simulations for the late 20th century. In central and northern Chile (17°–37°S) the most notable feature is a strong contrast between surface cooling at coastal stations (−0.2°C/decade) and warming in the Andes (+0.25°C/decade), only 100–200 km further inland. Coastal radiosonde data imply that the coast-Andes variation is largely due to strong vertical stratification of temperature trends in the atmosphere west of the Andes. The coastal cooling appears to form part of a larger-scale, La Niña-like pattern and may extend below the ocean mixed layer to depths of at least 500 m. Over continental Chile the CMIP-3 GCM ensemble predicts temperature trends similar to those observed in the Andes. The cooling along the Chilean coast is not reproduced by the models, but the mean SST warming is weaker there than any other part of the world except the Southern Ocean. It is proposed that the intensification of the South Pacific Anticyclone during recent decades, which is also a simulated consequence of global warming, is likely to play a major role in maintaining cooler temperatures off the coast of Chile.

Citation: Falvey, M., and R. D. Garreaud (2009), Regional cooling in a warming world: Recent temperature trends in the southeast Pacific and along the west coast of subtropical South America (1979–2006), *J. Geophys. Res.*, *114*, D04102, doi:10.1029/2008JD010519.

1. Introduction

[2] Since the late 1970s the mean temperature of the Earth's lower atmosphere has increased steadily, as has consensus within the scientific community that this behavior is largely attributable to anthropogenic greenhouse gas (GHG) emissions [*Hegerl et al.*, 2007]. The spatial patterns of temperature changes underlying global warming during this period have been highly nonuniform [e.g., *Trenberth et al.*, 2007], a result of both changes in atmosphere/ocean circulation related to the warming and the presence of natural modes of atmospheric variability whose amplitudes over interdecadal timescales are comparable to the anthropogenic signal. Along the west coast of South America (continental Chile), available records show temperature trends that are negligible or even negative at several sites, at odds with the mean global trend of around +0.33°C/decade [*Trenberth et al.*, 2007]. Many of Chile's water resources (especially its glaciers and snowfields) and industries (e.g., agriculture, fisheries, tourism) are significantly affected by temperature variability. Understanding the magnitude and spatial structure of recent temperature change, and reconciling these against expectations based on global warming, is therefore an important task. The intention of this article is to provide a comprehensive characterization of contemporary temperature trends in Chile (1979–2006), focusing particularly on their spatial patterns and vertical structure. To accomplish this we use a diverse collection of temperature data sets and draw insight from the results of general circulation model (GCM) simulations.

[3] A number of geographical and observational constraints make the characterization and interpretation of recent climate change in Chile a challenging but potentially rewarding task. The meridional extent of the country (~4000 km) ensures that it crosses several climatic regimes, from the hyperarid northern desert to the temperate, rainy south. In contrast, its zonal extent (150–250 km) is considerably less than the grid spacing of most observational analyses and global models and over these distances the surface topography may rise from sea level to over 6000 m. Long-term temperature records are scarce and not distributed optimally for separation of zonal, meridional, and vertical patterns. Chile's setting along

[1]Department of Geophysics, Universidad de Chile, Santiago, Chile.

0148-0227/09/2008JD010519$09.00

the coast of a large continental landmass means that both oceanic and continental variability may modulate local climate. Several large-scale modes of natural variability, most importantly the El Niño Southern Oscillation (ENSO), the Pacific decadal oscillation (PDO) and the southern annular mode (SAM), are known to strongly influence temperatures over interannual to interdecadal timescales [e.g., *Aceituno*, 1988; *Gillett et al.*, 2006; *Garreaud et al.*, 2008].

[4] Among the literature describing recent temperature variability in Chile, the work of *Rosenblüth et al.* [1997] is a standard reference. They examined annual temperature records for the period 1960–1992 and found significant warming (+0.14 to +0.38°C/decade) at several stations, the majority of which were located in the northern part of the country. They noted that most of the changes were due to increases in daily minimum temperatures, as was also observed by *Vincent et al.* [2005] and *Villarroel et al.* [2006] in indices of extreme temperatures for the period 1960–2000 and by *Rusticucci and Barrucand* [2004] over the adjacent Argentinean mainland (1958–98). Other studies have documented the vertical structure of temperature change [e.g., *Vuille and Bradley*, 2000; *Bown and Rivera*, 2007; *Boisier and Aceituno*, 2006], finding that high-altitude temperature trends may differ significantly from those at the surface. Many of the trends presented in the studies mentioned above are influenced by the widely documented climate regime change of 1976–1977 [e.g., *Trenberth and Stepaniak*, 2001; *Giese et al.*, 2002] that has been associated with significant shifts in mean temperature at many locations around the Pacific basin. *Boisier and Aceituno* [2006] examined temperature variability at several coastal sites in northern Chile. They noted that almost all of the warming in the period 1960–2000 actually occurred over a few years between 1975 and 1977 and that since this time trends have been weakly negative at all stations they considered. Marked temperature shifts in the middle to late 1970s are also evident at stations in central and southern Chile [e.g., *Rosenblüth et al.*, 1997; *Bown and Rivera*, 2007].

[5] This study focuses on the contemporary period from 1979 until 2006, after the climate shift of the mid-1970s and encompassing the satellite era during which the atmosphere and ocean have been sampled continuously with space based radiometers. A similar time period was chosen for the characterization of recent global temperature trends in the 2007 IPCC summary report, for essentially the same reasons [*Trenberth et al.*, 2007]. We make use of temperature data sets (both in situ observations and gridded analyses) that sample the land and sea surface, the upper atmosphere, and the ocean. These, along with a brief description of Chile's geoclimatic setting and the methodologies to be employed, are described in section 2. The core results of the paper are then presented in section 3, where we attempt to rationalize spatial variability in observed temperature trends. We examine patterns of change in the horizontal (i.e., meridional and zonal) and in the vertical and look for consistency among the different sources of temperature data. In section 4 we use GCM output to address whether the observed temperature trends are consistent with the predicted global warming response. In section 5 we summarize our key results and discuss their significance in the context of interannual variability within the Pacific Basin.

2. Study Area, Methodology, and Data

2.1. Study Area

[6] Because observational data is very sparse in the extreme south of Chile, our focus region (see Figure 3b) extends southward only as far as central Patagonia (i.e., from 17.5°S to 47.5°S). For the purposes of discussion, we divide the study area into three segments, each 10° wide, named northern (17.5°S–27.5°S), central (27.5°S–37.5°S), and southern (37.5°S–47.5°S). The climate of each of these regions may be loosely described as arid, Mediterranean, and rainy, respectively. The eastern border of Chile follows the ridge of the Andes mountain chain, whose height varies from over 5000 m in the north to under 2000 m in the south. In central Chile a coastal mountain range, about 1000–1500 m high, runs north–south about 50 km inland. The region between this and the Andes is referred to as the "central valley."

2.2. Methodology

[7] The main variable that this article will deal with is the linear trend of annual mean temperature over the 28 year period from 1979 to 2006, calculated using standard least squares regression. As a general rule, all tendencies presented in this article are required to be based on at least 20, nearly complete (>85%), years of data. Mean trends are occasionally calculated for groups of stations and in these cases the trends are derived from a single series of station averaged annual mean temperatures.

[8] Statistical significance is presented as a 90% confidence interval, based on a 1000 member synthetic null distribution derived by randomly reordering the annual series. The confidence limits do not take into account possible systematic errors in observational data or autocorrelation in the series. We emphasize that the word "significant" should be interpreted in a purely statistical sense, i.e., that a random series of data with the same variability would be 90% likely to have a smaller absolute trend and does not necessarily mean that the trend is representative of a physically significant process (such as one related to global warming, for example).

2.3. Observational Data Sets

[9] The key characteristics of the in situ and gridded data sets to be used are summarized in Tables 1 and 2, respectively. All data sets begin at or before 1979, but not all extend until 2006. Detailed description of the processing methodologies, uncertainties, and caveats associated with each of these data sets is beyond the scope of this article. What follows is a brief discussion of what we deem to be the most important issues, and further information may be obtained in the references provided in Tables 1 and 2.

2.3.1. In Situ Data

[10] Our principal data set is derived from recently digitized long-term records of daily maximum and minimum temperature at 20 sites maintained by the national weather service (Direccion Meteorológica de Chile (DMC)). Daily mean temperatures were estimated by taking the average of the daily maximum and minimum. The DMC

Table 1. In Situ (Station) Time Series of Temperature Obtained From Both Local and International Institutions[a]

Name	Source	Number of Sites	Last Available Year	Variable	Interval	Reference
Chile Synop	DMC	20	2006	T_{max}, T_{min}	Daily	*Villarroel et al.* [2006]
Lagunitas	Andinas Mine	1	2002	T_{mean}	Daily	
El Yeso	Aguas Andinas	1	2006	T_{mean}	Monthly	
GHCN	NOAA	10	2006	T_{mean}	Monthly	*Peterson and Vose* [1997], *Peterson et al.* [1998]
Radiosonde	DMC	3	2005: Antofagasta, P. Montt; 1998: Quintero	*T*	Daily (1200 UTC)	*Boisier and Aceituno* [2006]
Coastal oceanographic	SHOA	6	2006	*SST*	Monthly	

[a]The specific temperature variables vary among the data sets. They include the instantaneous temperature (T), the daily maximum (T_{max}) and minimum (T_{min}), the time averaged (daily or monthly) temperature (T_{mean}) and sea surface temperature (SST). DMC, Dirección Meteorológica de Chile (National Weather Service); GHCN, Global Historical Climatology Network; SHOA, Servicio hidrográfico y oceanográfico de la armada (Navy oceanographic and hydrographical service); NOAA, National Oceanic and Atmospheric Administration.

stations provide a reasonable sampling of Chile in the meridional direction, but sampling in the zonal direction is somewhat inadequate (e.g., Figure 3b). In northern Chile the sites are mostly coastal, while in central Chile they are generally situated inland at several hundred meters above sea level. In southern Chile most sites are low-lying, and three (Balmaceda, Cochrane, and Chile Chico) are in the lee of the Andes. Sites at high altitudes in the Andes are rare. In the DMC network there is only Calama, in northern Chile, at 2300 m above sea level. To go some way toward improving data coverage, temperature records (available from the early 1970s) were also acquired for two privately operated sites in the Andes of central Chile: Lagunitas (2600 m) and El Yeso (2400 m). Monthly surface temperature measurements from the global historical climatology network (GHCN) provide further long-term data at several stations on the eastern side of the Andes. A network of tide gauges maintained by the Chilean Oceanographic and Hydrographic Service (SHOA) provide long-term records of sea surface temperature (SST) along the coast of central and northern Chile (Figure 3b).

[11] Coastal upper air data are available from three rawinsonde stations (also operated by the DMC) near the central parts of northern (Antofagasta, 23.5°S), central (Quintero, 33°S), and southern (Puerto Montt, 42°S) Chile, where soundings are made regularly at 1200 UTC (0800 local time). The temperature data are recorded on standard pressure levels and on variable significant levels, chosen so as to provide an adequate representation of the vertical temperature structure. The data were hydrostatically interpolated onto a 100 m spaced height grid.

[12] All in situ data sets have missing observations and different strategies were adopted to mitigate their effect on trend estimations. In the case of the daily surface temperature data sets, gaps of 3 days or less were filled by linearly interpolating between surrounding data points. Longer gaps, and missing months from the monthly data, were filled with climatological values calculated for the period 1979–2006. Missing upper air data were replaced with 1200 UTC temperatures interpolated from NCEP-NCAR Reanalysis [*Kalnay et al.*, 1996]. Overall, the trends calculated with these data replacement strategies were not significantly different to the trends calculated by simply ignoring missing data.

2.3.2. Gridded Analyses

[13] Our study employs global gridded analyses of surface air temperature from the National Climatic Data Center (NCDC) and the extended-reconstructed (ERSST) and Hadley Center (HadISST) sea surface temperature analyses. Upper-air temperatures were obtained from the microwave sounding units (MSU) on National Oceanic and Atmospheric Administration (NOAA) polar-orbiting satellites. Available since 1978, these measurements provide estimates of bulk temperatures in several atmospheric layers. Here we use midtroposphere (channel 2) data, which may be interpreted as the mean temperature within a broad region of the midtroposphere, with maximum weighting between 4 and 7 km above the surface [*Mears et al.*, 2003]. Although the MSU data set has been a source of some controversy in the

Table 2. Global Analyses of Temperature and Sea Surface Temperature[a]

Name	Source	Original Data/Instrument	Last Available Year	Variable	Frequency/Resolution	Reference
NCDC Surface	NOAA	GHCN (land) ICOADS (sea)	2006	*T* (surface)	Monthly/5°	*Smith and Reynolds* [2004]
ERSST (V2)	NOAA	ICOADS	2006	*SST*	Monthly/2°	*Smith and Reynolds* [2004]
MSU	RSS	Satellite Microwave Radiometer	2006	*T* (troposphere)	Monthly/2.5°	*Mears et al.* [2003]
Ocean Heat Content	NODC	WOD05	2003	*T* (ocean)	Annual/1°	*Levitus et al.* [2005]
HadISST	Hadley Center	GTS/ICOADS	2003	*SST*	Monthly/2°	*Rayner et al.* [2003]

[a]T_{mean}, temperature; SST, sea surface temperature; RSS, Remote Sensing Systems; GHCN, Global Historical Climatology Network; ICOADS, International Comprehensive Ocean Atmosphere Data set; WOD05, World Ocean Database version 5; GTS, Global Telecommunications System; NOAA, National Oceanic and Atmospheric Administration; NODC, National Oceanographic Data Center.

climate change debate [*Wallace et al.*, 1999], the version used in this study is generally accepted as being representative of large-scale temperature changes and is consistent with global analyses of temperature change from radiosonde observations [*Mears et al.*, 2003]. Owing to difficulties in modeling of the diurnal range of high-altitude surface emissions, we consider the MSU data to be unreliable where the surface topography is higher than 1000 m, including the Andes of central and northern Chile.

[14] Analyses of subsurface ocean temperature were obtained from the ocean heat content database of *Levitus et al.* [2005], a gridded analysis of temperature anomalies at several depths from the surface to 3000 m, based on hydrographic observations from the World Ocean Database (WOD) [*de Boyer Montégut et al.*, 2004]. Global and hemispherical ocean heating estimates have been successfully derived from this data set [*Levitus et al.*, 2005; *Gille*, 2008], but regional estimates of long-term temperature variability must be treated with caution as data availability is poor in many areas. A recent study [*Gouretski and Koltermann*, 2007] has shown that the Levitus data set may suffer from a bias toward cooling trends due to the introduction of erroneous expendable bathythermograph (XBT) data. In this study, the WOD data is used to estimate annual ocean temperature trends in rectangular sections 5°E–W and 10°N–S off the coast of northern, central, and southern Chile. Uncertainty due to uneven data sampling is a major issue. During some years only a few observations were available, and in others, several hundred. We compared the series of annual mean temperature variability at the surface level with SST series derived from the ERSST and HadISST data sets and found significant correlations (r = +0.6) and similar trends (see section 3). This gives us some confidence that the WOD data may provide a useful description of ocean temperature variability along the Chilean coast.

2.4. Climate Model Ensemble

[15] General circulation model (GCM) data were obtained from the World Climate Research Programme's (WCRP's) Coupled Model Intercomparison Project phase 3 (CMIP3) multimodel data set, produced for the Fourth Assessment Report (AR4) of the Intergovernmental Panel on Climate Change (IPCC). At the time this study was carried out, the CMIP3 database contained surface air temperature and SST output from 21 coupled ocean-atmosphere models for several GHG emissions scenarios. Outputs from two climate simulation experiments are considered: The 20C3m (Climate of the 20th Century) simulations span the period 1900–2000 and are forced by the observed history of GHG (anthropogenic and non-anthropogenic) and solar activity. The SRESA2 simulations extend from 2000 to 2100 under the hypothetical A2 emissions scenario [*Nakicenovic et al.*, 2000]. The SRESA2 scenario serves to most clearly identify anthropogenic climate trends as the greenhouse gas forcing is stronger than the 20C3m or any of the other 21st century scenarios with the exception of the A1F1 scenario (for which less data is available). Many models provide multiple realizations (runs) of the climate scenarios. Before calculating multimodel statistics (such as mean trends) the data from individual runs are first averaged for each model in order to prevent the statistics from being unduly weighted toward those models that provide a large number of runs.

3. Temperature Tendencies

3.1. Global Context

[16] In order to provide a large-scale context for our description of recent temperature trends in Chile, we first consider the global patterns of surface and midlevel temperature change using the gridded NCDC/ERSST/HadISST and MSU data sets (Figure 1). During the period 1979–2006 surface warming (Figure 1a) has been near ubiquitous over continental areas. Over the oceans, the ERSST product (Figure 1a) shows significant positive SST trends in the North Atlantic, most of the Indian Ocean, and the tropical and subtropical western Pacific, while weak cooling trends are observed over much of the eastern equatorial Pacific. Cooling also prevails over the Southern Ocean in a near-circumpolar pattern interrupted by a region of strong warming over and to the east of the Antarctic Peninsula. The SST trends from the alternative HadISST product (Figure 1b) shows a similar large-scale pattern, although there are often substantial regional-scale differences between the ERSST and HadISST products. In the midtroposphere (Figure 1c), the MSU data show a more homogenous pattern of heating and cooling, with much less contrast between continental and oceanic regions. In the Southern Hemisphere (SH), significant warming trends in the tropics and subtropics give way to significant cooling trends at higher latitudes, with the inflexion point at around 40°S on zonal average.

[17] The patterns of warming and cooling over the tropical and subtropical Pacific bear a marked resemblance to the canonical spatial structures associated with Pacific decadal variability (PDV) of SST [e.g., *Mantua et al.*, 1997; *Montecinos and Pizarro*, 2005; *Burgman et al.*, 2008]. The spatial fingerprint of the SST anomalies related to PDV are similar to the El Niño patterns for interannual variability, although they are strongest at subtropical (rather than tropical) latitudes [e.g., *Zhang et al.*, 1997; *Power et al.*, 1999; *Garreaud and Battisti*, 1999; *Burgman et al.*, 2008; *Chen et al.*, 2008]. From 1979 to 2006 most measures of interdecadal variability in the Pacific exhibit a decreasing trend [*Trenberth et al.*, 2007; *Chen et al.*, 2008]. Consistently, the SST trend pattern over this period shows a distinctly La Niña-like structure.

[18] We focus now on southern South America, where Chile sits squarely along the interface between a cooling ocean and warming continent (Figure 1a). The contrast is strongest in central and northern parts of the country, where the SST cooling is around −0.2°C/decade near the coast, while the continent immediately to the west has been warming by roughly the same amount. The offshore cooling extends along most of the west coast of South America and forms part of a crescent shaped pattern that connects the circumpolar cooling in the Southern Ocean with the cooling region in the eastern equatorial Pacific. This structure is also evident in the HadISST data (Figure 1b), although the southern branch of the cooling pattern is less well defined.

3.2. Horizontal Structure

[19] The coarse resolution of the gridded data sets in Figure 1 prevents any clear identification of regional vari-

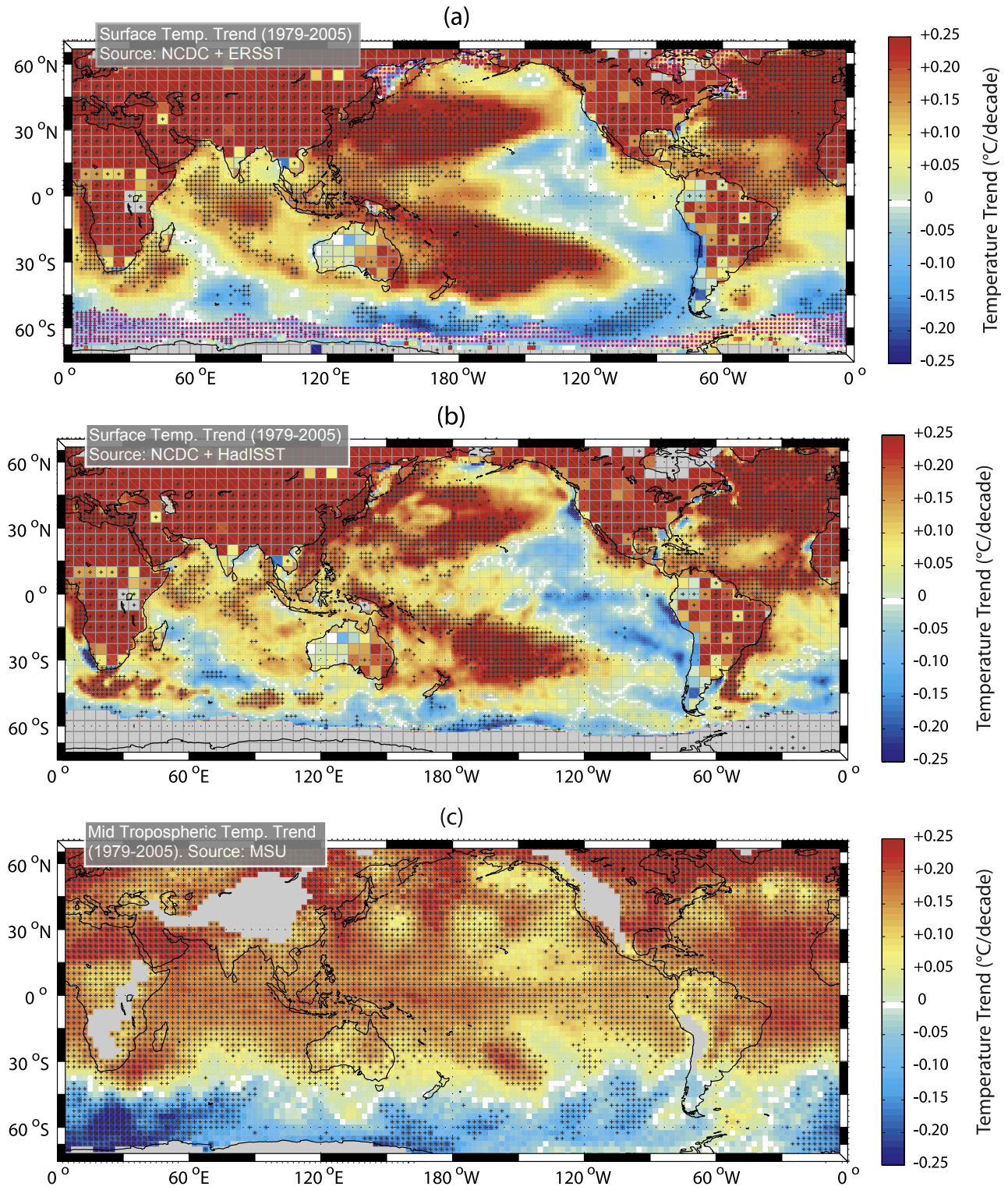

Figure 1. Global trends of (a, b) surface and (c) midtroposphere temperatures for the period 1979–2006. The surface temperatures are taken from the NCDC data set at 5° spacing, replaced over ocean areas by the higher resolution ERSST (2° spacing) (Figure 1a) and HadISST (1° spacing) (Figure 1b) data sets. Note that over coastal grid points the NCDC data may include a combination of ocean- and land-based observations. The midtroposphere data are derived from the 2° spaced MSU data set. MSU trends are not calculated for grid cells where the mean topography is higher than 2000 m. The color scale of the plot is chosen to emphasize the spatial structure of the trends in the vicinity of Chile and is deliberately saturated in some parts of the world (such as the Northern Hemisphere continents, for example). Dark crosses indicate grid points where trends are estimated to be 90% significant. Purple crosses indicate grid points that were covered by sea ice during at least 1 month of the period considered.

ation within Chile itself. In particular, it is unclear from this data if the continental warming extends westward past the Andes, or if the cooling observed over the ocean surface penetrates further inland. To address this question we turn to the local surface temperature data. Figure 2 shows time series of the annual mean temperature anomalies for all available stations in central Chile, where observational coverage is highest. The stations are grouped into geographic zones that form a rough transect from the offshore Juan Fernandez Island (bottom) to the eastern side of the Andes (top). The time series, which begin in 1960, clearly demonstrate the abrupt change in mean temperature associated with the 1976/1977 regime shift, particularly at sites nearer to the coast. During the focus period of this study (1979 onward) there is no visual evidence of any further regime changes or other significantly nonlinear behavior. The station data do show systematic trends during this period, the most striking aspect of which is the rapid reversal in sign that occurs between the coast and the Andes. At Juan Fernandez Island (~800 km offshore) the temperature series has a significantly negative trend (-0.18 ± 0.11°C/decade). A weakly (but not significantly) negative trend (-0.12 ± 0.3°C/decade) is also present at the coastal sites (Figure 2d). However, less than 150 km inland in the central valley (Figure 2c) the sign of the trend has reversed and is significantly positive ($+0.18 \pm 0.14$°C/decade). The warming is even stronger in the western Andes ($+0.28 \pm 0.34$°C/decade), although strictly speaking this value is not quite significant due to high interannual variability (partly due to data quality issues). A similar positive trend ($+0.23 \pm 0.24$°C/decade) is observed on the eastern side of the Andes in the continental interior.

[20] In Figure 3a temperature trends from all stations in the study area are plotted as a function of latitude. The Chilean surface stations are separated into two groups: low-lying (usually coastal) stations below 150 m altitude and elevated (always inland) stations at higher altitudes. Coastal SST trends derived from the SHOA stations and the two gridded SST products (ERSST and HadISST) are also included. Owing to the short time period considered and high interannual temperature variability (especially in northern Chile where ENSO is most influential) the uncertainty ranges of most trend estimates are large. Nonetheless, in central and northern Chile there is a good correspondence among the different sources of coastal data, which generally indicate cooling rates between -0.1 and -0.3°C/decade. Weakly positive trends are indicated by the HADISST data between 25° and 20°S, but these do not agree with either the in situ data or the ERSST product at these latitudes. The strong contrast between coastal cooling and inland warming is seen to extend into northern Chile, where inland sites register positive trends of +0.2 to +0.25°C/decade. In northern Chile most of the inland sites are on the eastern side of the Andes. However, the significant warming of $+0.25 \pm 0.2$°C/decade at Calama provides a key fragment of evidence that the warming observed in the western Andes of central Chile may extend northward at least as far as this station (23°S). *Vuille and Bradley* [2000] noted significant positive trends on the western side of the tropical Andes (22°S–0°S; 1959–1998), suggesting that the warming pattern may in fact encompass the length of the western side of the subtropical and tropical Andes. However, the applicability of this result may be questionable as it includes the 1976–1977 climate shift and may not be representative of the period examined in this study.

[21] In southern Chile most temperature trends are close to zero at coastal and inland sites alike, and no obvious meridional structure is evident. There are no high-altitude stations (>2000 m) comparable to those in central and northern Chile (partly because the height of the Andes decreases rapidly at latitudes higher than about 35°S), and the southward extent of the Andean warming cannot be determined. The station distribution in southern Chile is not ideal for determining east-to-west patterns in the temperature trends. Although there are no in situ observations, both of the gridded data sets indicate that the SST cooling is present in southern Chile, although somewhat weaker than in the north.

3.3. Vertical Structure

[22] Owing to the rapid change in topographic elevation from the coast to the Andes, the strong contrast between ocean cooling and warming inland is interpretable as a change in temperature trends with altitude. Figures 4a–4c provide another visualization of the temperature trends, this time as a function of elevation. All observational data sets are incorporated, including the radiosonde profiles and ocean temperature analysis. This assemblage of data allows temperature tendencies from multiple data sources to be plotted from 700 m below to 10 km above sea level.

[23] The radiosonde data show a transition in the mid-troposphere from warming in the north (Antofagasta) to cooling in the south (Puerto Montt). The cooling at Puerto Montt is weak (-0.1°C/decade) and roughly uniform from the surface to 10 km. In the central and northern sectors (Quintero and Antofagasta) the trends exhibit significant, and similar, vertical structure. Both show cooling near the surface, consistent with coastal surface temperature and SST measurements. At Quintero the strongest cooling occurs at the surface level, while at Antofagasta the maximum cooling trend (-0.43°C/decade) is at 600 m. Above these levels the trends increase rapidly, switching over from cooling to warming at heights of 500 m (Quintero) and 1000 m (Antofagasta), and peaking at about 1300 m at both locations, where warming rates are +0.35 and +0.5°C/decade, respectively. Above, the warming trends slowly decrease, but remain positive throughout the column at Antofagasta. At Quintero, temperature tendencies actually become weakly (but not significantly) negative between 4000 and 7000 m.

[24] The lower troposphere along the north-central coast of Chile features a cool, moist marine boundary layer (MBL), often topped by stratocumulus (Sc), and capped by a temperature inversion maintained by subsidence. In Antofagasta (Quintero) the MBL is about 800 m (300 m) deep and present about 90% (50%) of the time [*Boisier and Aceituno*, 2006]. The differential temperature trends near the surface and further aloft observed in Quintero and Antofagasta have important implications for the MBL-inversion structure. In both locations, the cooling encompasses the whole MBL and the inversion base while the warming is greatest near the inversion top, thus increasing the inversion strength and the lower tropospheric stability (LTS). In a climatological context an increase of LTS has

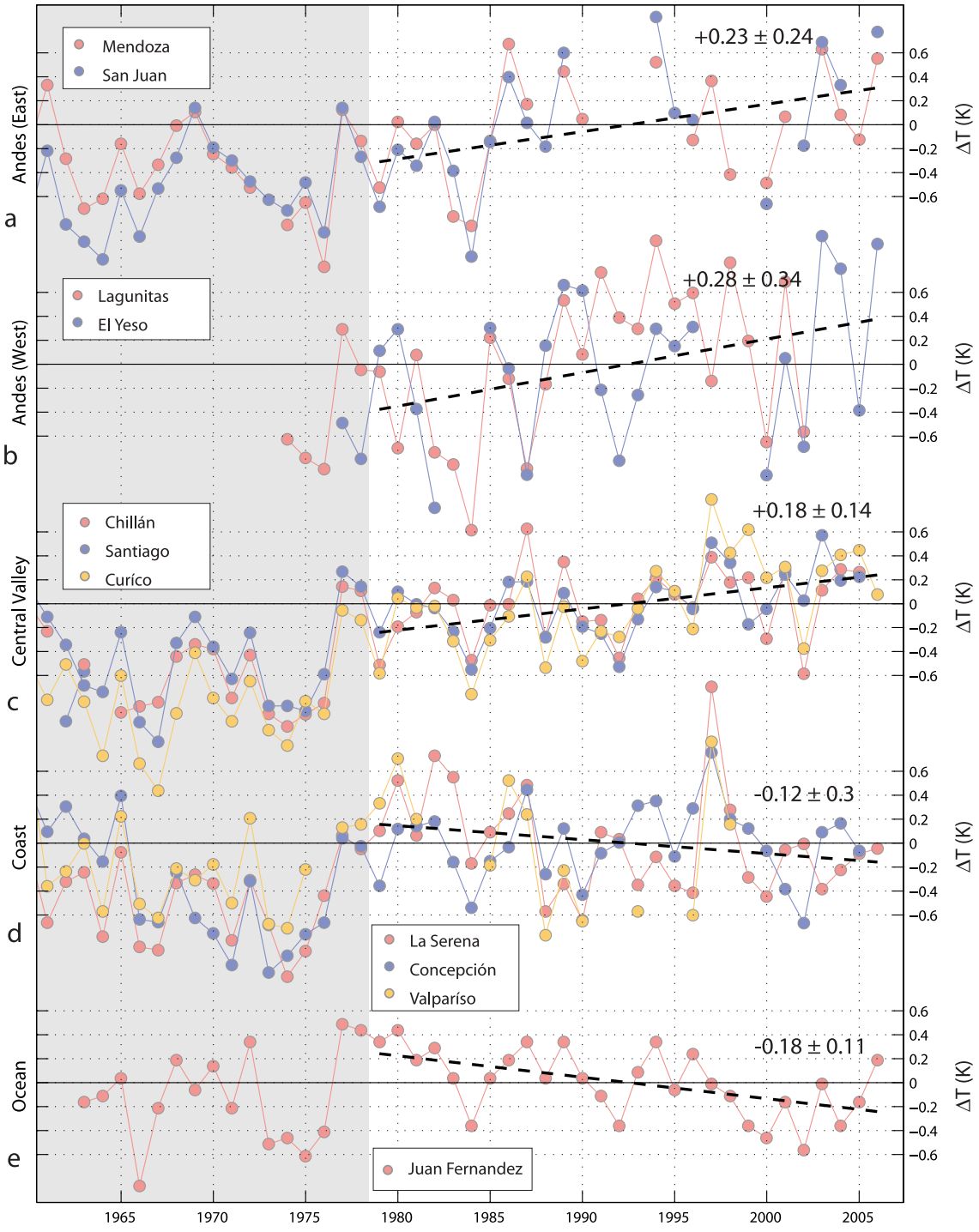

Figure 2. Time series of surface atmospheric temperature anomalies (ΔT) in central Chile (27.5°–37.5°S). Anomalies are calculated with respect to the period 1979–2006. Stations are divided into five geographic zones, which are (from bottom to top): (e) ocean, (d) coast, (c) central valley, (b) western Andes, and (a) eastern Andes. Data from a station at Valparaiso are included in the central plot, although due to the large amount of missing data trends they are not calculated for Valparaiso elsewhere. The dashed lines show the linear fit to the data in each group for the period 1979–2006, calculated from the annual mean ΔT from all stations in each group. The associated trends, along with the 90% confidence interval, are also provided. Gray shading identifies years prior to 1979.

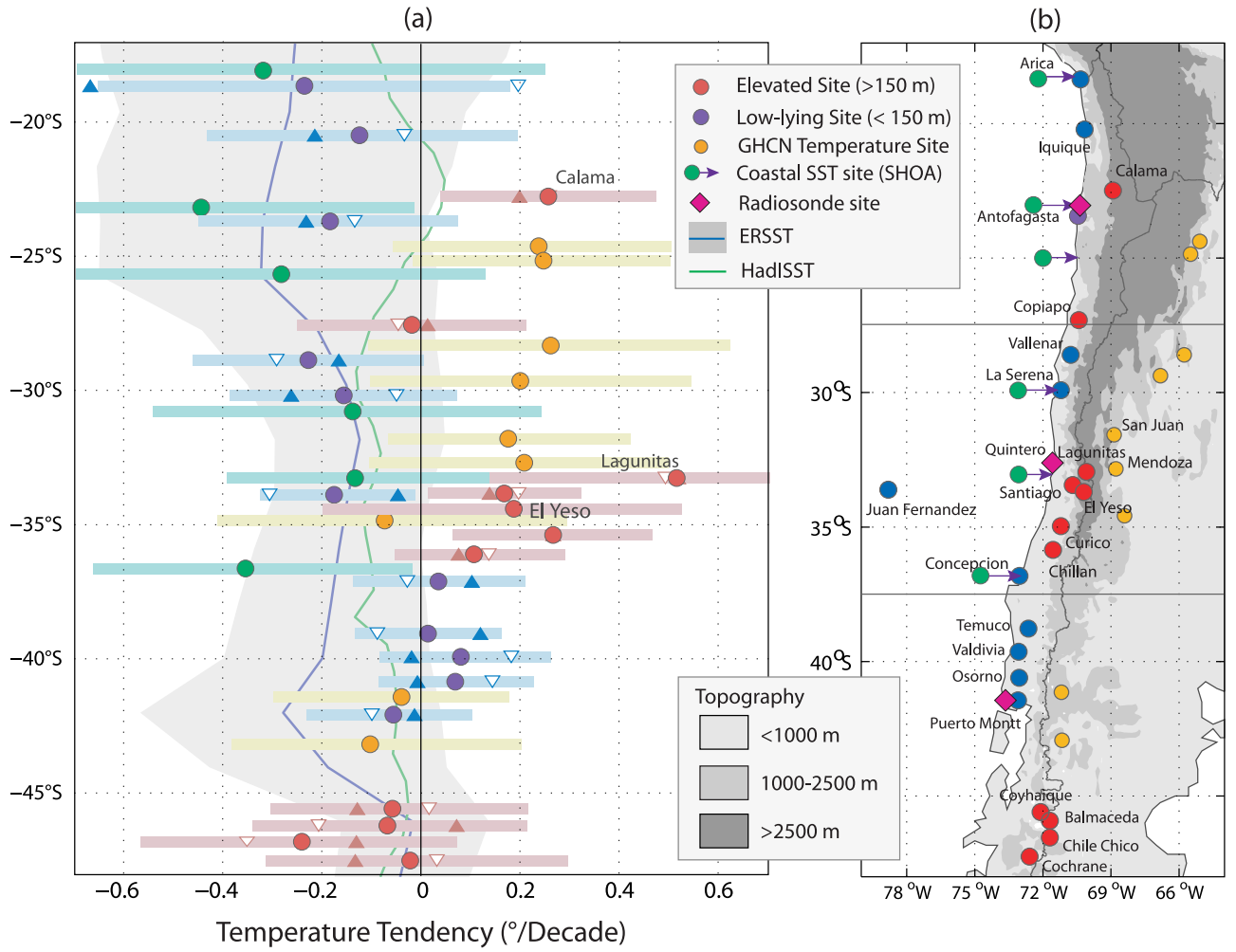

Figure 3. Meridional variation of trends in daily mean temperature for the period 1979–2006. (a) Circles indicate temperature trends, plotted against station latitude, derived from the data sources indicated in the legend at the top right. Stations in Chile are divided into low-lying (<150 m) and elevated (>150 m) sites. The solid bars represent 90% confidence intervals. Solid upward facing and open downward facing triangles indicate trends in the daily maximum and daily minimum temperature, respectively. The vertical positions of the symbols have in some cases been adjusted slightly so as to clearly separate stations at similar latitudes. The blue and green lines indicate trends from the coastal grid points of two alternative SST analyses (ERSST and HadISST). The solid gray region indicates the 90% confidence for ERSST. (b) The locations of station data.

been associated with an increase in Sc cloud amount [e.g., *Klein and Hartmann*, 1993] but the long-term trends in available cloud data in northern Chile have not yet been studied in detail.

[25] The trends obtained by the radiosonde data fit well with those derived from surface observations, implying that the variation between the coast and the Andes is largely representative of the vertical structure of trends in the free atmosphere. For example, the warming above the MBL at Antofagasta is near identical to that registered at the same altitude at Calama, some 150 km inland. The same is true in central Chile, where the warming trends at the inland stations (e.g., El Yeso, Lagunitas, Santiago, Chillan) are comparable to the positive trends exhibited by the radiosonde data within the same altitude range. Furthermore, the transition in the midtroposphere from warming in the north to cooling in the south (Puerto Montt) is broadly consistent with the large-scale zonal pattern suggested by the MSU data (Figure 1b). The consistency between the different data sets is noteworthy given that several past studies have shown that the climatological characteristics (including trends) of surface temperatures at elevated sites in other parts of the world often differ significantly from those at the same altitude in the surrounding free-troposphere [e.g., *Seidel and Free*, 2003; *Pepin and Seidel*, 2005].

[26] The vertical profiles of Figure 4 include below the sea surface (OHC) temperature tendencies averaged over the regions defined in Figure 3b. For reference, the SST cooling from the ERSST data set averaged over the same regions is also plotted. At the surface, the trends are consistent with the SST data. In each of the three areas the cooling trends extend downward to depths of 250 m in the south, and 500 m in the central and northern zones, well below the mixing layer depth of ~50 m [*de Boyer Montégut*

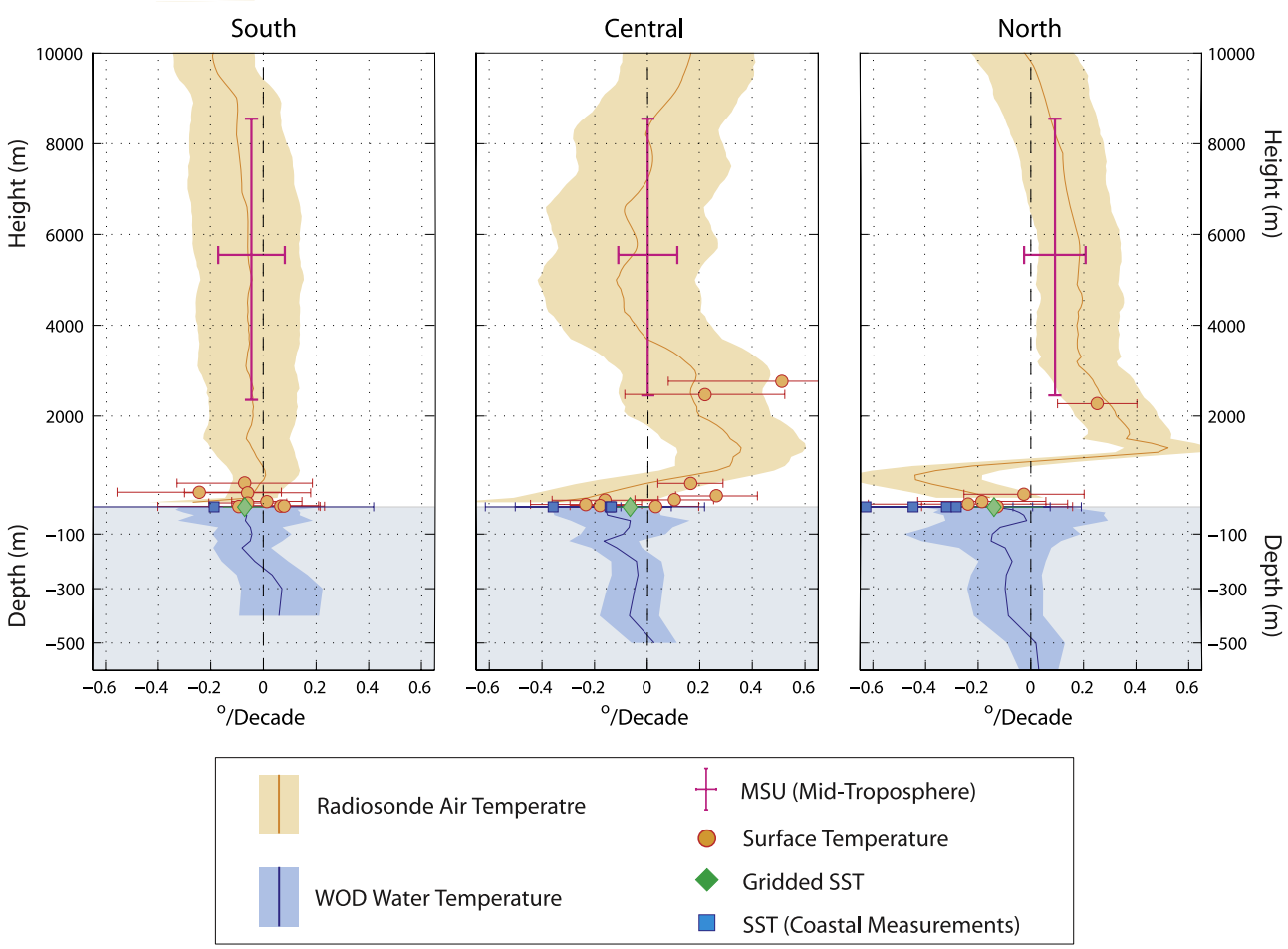

Figure 4. Vertical profiles of temperature trends in (a) southern, (b) central, and (c) northern Chile. The upper portion of each graph (white background) represents the atmosphere and the lower (blue background) portion represents the ocean. The solid orange lines are radiosonde derived trends at 100 m intervals, the lighter shaded region indicating the 90% confidence interval. The radiosonde stations are Puerto Montt (south), Quintero (central), and Antofagasta (north). The pink bars represent midtropospheric trends from the MSU data set, horizontally interpolated to the station, and plotted at a representative altitude of 5500 m. Orange circles and blue squares represent temperature trends derived from the in situ measurements of T and SST. The green diamonds show the mean SST trends in each 10° region between the coast and 75°W. Ocean temperature trends (blue lines) from WOD data averaged within the same regions are shown from the surface to 700 m depth. The blue shading indicates the 90% confidence level.

et al., 2004]. Owing to the very large systematic uncertainties and sampling problems associated with the OHC analyses we do not wish to draw too much attention to these results, but it is nonetheless of interest to note that the coastal cooling may not be restricted to the near surface, but might instead extend to deeper waters below the mixed layer.

3.4. Extreme Temperatures and Seasonal Means

[27] So far we have concentrated on the spatial patterns of daily mean temperature trends. However, several past studies [e.g., *Rusticucci and Barrucand*, 2004; *Vincent et al.*, 2005; *Villarroel et al.*, 2006] have noted that trends in daily maximum (T_{max}) and minimum (T_{min}) temperatures may be significantly different. In Figure 3a the trends in T_{max} and T_{min} are presented at sites where daily extreme data are available. In general, the trends in temperature extremes fall within the 90% confidence intervals of those for the daily mean. In the north, most coastal stations show stronger negative trends for T_{max}. At Arica (the northernmost station considered), the T_{max} and T_{min} trends are of opposite sign and fall outside the 90% confidence interval (the only station where this occurs). The differences between the trends of T_{max} (more strongly decreasing) and T_{min} (less strongly decreasing) suggests that the trends at coastal sites are strongly modulated by the cooling of the nearby ocean, since the low-level atmospheric flow in central and northern Chile is usually onshore during the day (bringing oceanic air to the station), and weakly offshore at night [*Rutllant and Ulriksen*, 1979]. The stronger T_{max} cooling contrasts with what occurred during the climate shift of 1976–1977, when the mean minimum temperatures increased dramati-

cally at many stations in northern Chile (see also *Villarroel et al.* [2006]). The high-altitude site Calama shows no notable difference in the trend for T_{max} and T_{min}, and neither do the inland stations in central Chile. In the south the trends in T_{max} and T_{min} are often quite different, and sometimes of opposing sign, but no clear meridional pattern can be identified.

[28] When separated into seasons the spatial patterns of temperature trends (not shown) remain qualitatively similar to those presented in Figures 3–4, and seasonal trends are rarely outside of the 90% confidence range of the annual mean data. Both the coastal SST and the majority of surface stations show slightly stronger cooling during the summer semester, from December to May. The semicircular cooling pattern in the SST off the Chilean coast is also most pronounced during summertime and is clearly situated around the eastern edge of the South Pacific Anticyclone (this is discussed further in section 4). In winter, the SST cooling in the southeast Pacific is weaker, has less spatial structure, and shows no clear relationship to the mean low-level circulation pattern.

4. Insight From Global Circulation Models

[29] In this section we make use of the (CMIP-3) multi-model GCM ensembles to examine to what extent the observed regional temperature variability can be interpreted as a consequence of greenhouse gas forcing. Model results from the last 28 years of the 20C3m experiment (1972–2000) are taken to be representative of the observational period (1979–2006) examined for this study. An assumption in our analysis is that climate change patterns common to the majority of the models should represent a response to external forcing, since other modes of internal variability (if any) should cancel out after calculating the ensemble average [e.g., *Cai and Cowan*, 2006]. Because the 20C3m scenario includes emissions from both natural and anthropogenic sources, along with observed solar activity, trends in these simulations cannot be uniquely attributed to anthropogenic forcing.

[30] The mean temperature trends simulated by the CMIP-3 ensemble are shown in Figure 5 for the near surface (Figure 5a) and midtroposphere (Figure 5c). These plots are roughly analogous to the NCDC/ERSST and MSU trends plotted in Figures 1a, 1b, and 1c, respectively. The warming pattern is quite homogeneous over most of the globe. At the surface spatial variability is mostly determined by the well known contrast between oceanic and continental trends [i.e., *Trenberth et al.*, 2007]. In the SH, weaker warming at both the surface and upper levels is simulated at middle and high latitudes (Figures 5b and 5d), and the zonal mean trend is effectively negligible south of 60°S. The slower warming rate over the Southern Ocean is expected due to the strong mixing and upwelling beneath the Antarctic circumpolar current [e.g., *Russell et al.*, 2006] and although the ensemble mean does not reproduce the cooling that is actually observed (except for a small region south of New Zealand), several of the underlying models do indicate significant negative trends (Figure 5d). This has lead several authors to suggest that the high-latitude cooling in the Southern Hemisphere (often associated with a well documented increasing trend in the SH annular mode) is ultimately a consequence of a combination of ozone depletion in the polar stratosphere and increasing tropospheric GHG concentrations (e.g., *Gillett and Thompson* [2003], *Cai et al.* [2005], and *Miller et al.* [2006], among others).

[31] Over the Pacific Ocean, the La Niña-like patterns, including the tongue of cooling along Chile's coast, are largely absent in the model ensemble mean. It has been suggested [e.g., *Cane et al.*, 1997; *Cook et al.*, 2007] that a tendency toward a more La Niña-like state should result from global warming in accord with the Bjerknes feedback mechanism [*Bjerknes*, 1969; *Clement et al.*, 1996]. However, other researchers have suggested that more El Niño like conditions might be expected due to a weakening of the tropical circulation [e.g., *Held and Soden*, 2006; *Vecchi et al.*, 2006]. The response of the tropical Pacific to global warming thus remains very much an open question [*Vecchi et al.*, 2008]. The results from the CMIP-3 ensemble, which show no clear La Niña- or El Niño-like tendency, provide little support for either idea [see also *Collins and the CMIP Modelling Groups*, 2005]. Along the Chilean coast, the GCM ensemble mean trend is positive over both land and sea, although, as at other land-sea interfaces, the warming rates are considerably higher over the continental areas. Figure 6 plots the coastal temperature against the inland temperature of central Chile (approx 30°S) predicted by each GCM. Although there is considerable scatter among the different predictions, all but four of the simulated temperature trends fall within the positive quadrant of the graph, indicating simultaneous warming in both regions. The ensemble average tendency in the Andes of +0.26°C/decade compares very well with the observed value of (roughly) +0.25°C/decade. However, none of the models show an ocean cooling trend near to that observed, and across the models there is a strong positive correlation between trends over the ocean and Andes. Thus the few models that do show negative temperature trends over the ocean are also those that show the lowest trends in the Andes.

[32] Although it is clear that none of the models are able to reproduce the opposite temperature trends between coast and continent, it is notable that they do predict less warming off the coast of Chile than over the rest of the tropical and subtropical oceans. Indeed, warming rates off the Chilean coast are weaker than in any other part of the world except for the Southern Ocean. When comparing spatial patterns of temperature change it is useful to express the SST trends as anomalies with respect to the global mean trend. In Figure 7 we compare the anomalous trends in the South Pacific derived from observations (ERSST) (Figure 7a) and the CMIP-3 GCM ensemble (Figure 7b). Because extratropical SST variability is known to be strongly related to the low-level atmospheric circulation over all timescales [e.g., *Kushnir et al.*, 2002], the observed (NCEP/NCAR Reanalysis) and GCM ensemble mean sea level pressure (SLP) trends are also included in Figure 7.

[33] To the west of the coast of Chile the GCMs (Figure 7b) show a robust region of negative SST trend anomalies (about −0.07°C/decade below the global mean) that bears a tangible resemblance to the observed crescent shaped cooling pattern (Figure 7a), albeit with a considerably smaller amplitude and no tropical signal. In both cases, the regions of relative cooling curl around the eastern side of positive

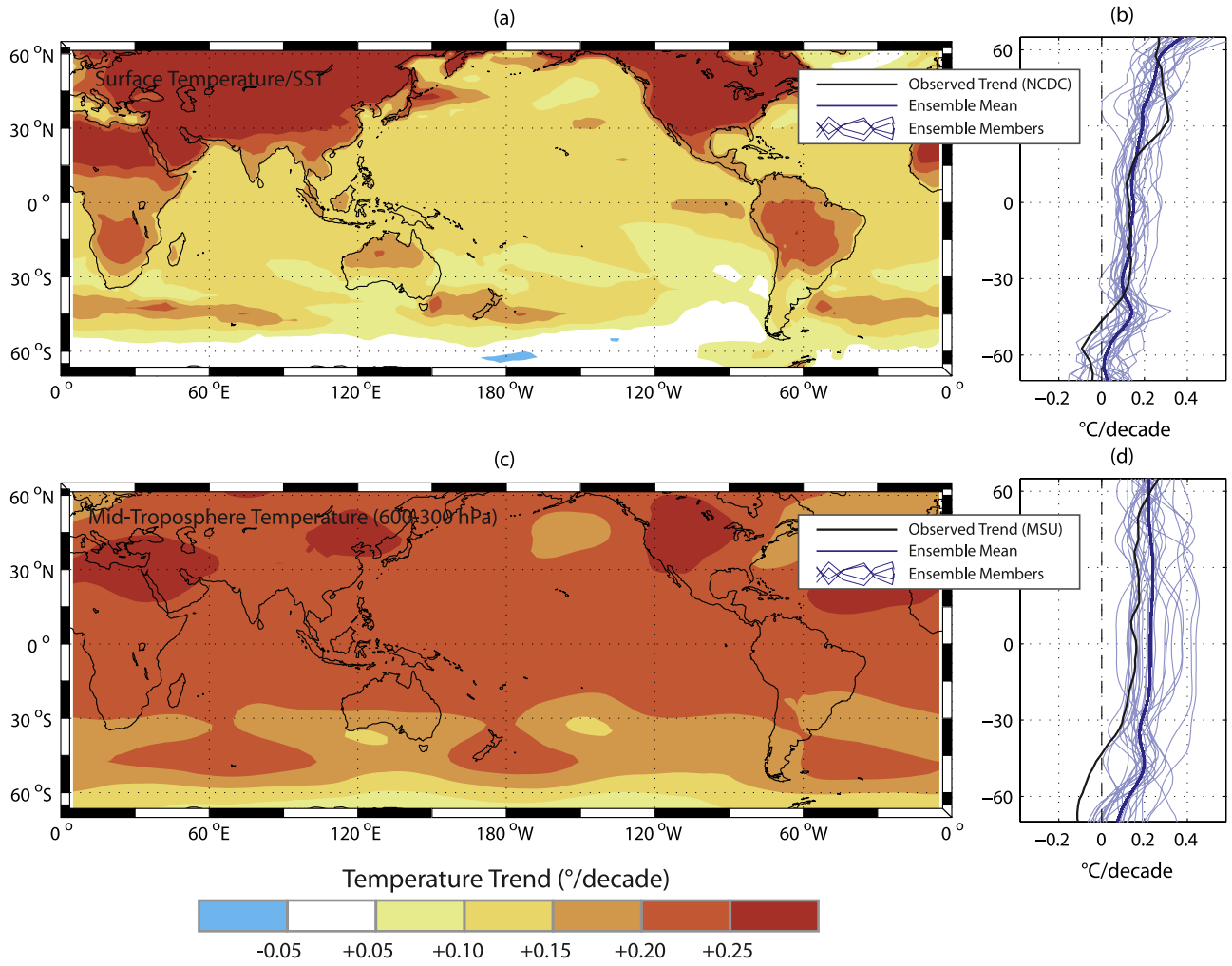

Figure 5. Ensemble mean (a) surface and (c) midtroposphere temperature trends from the CMIP-3 multimodel data set for the last 3 decades of the 20th century (1972–2000). Model data were interpolated onto a common 2.5° spaced grid before calculating trends. The midtroposphere temperature is defined as the mean temperature between 700 hPa and 300 hPa, roughly analogous to the atmospheric layer sampled by the MSU instrument (Figure 1b). (b, d) The zonal mean temperature trends from the individual models (thin blue lines) and the ensemble mean (blue solid line). The black lines show the zonal mean vales of the observed trends from NCDC (surface) and MSU data sets.

pressure trend anomalies. In the observations, the SLP trends are roughly colocated with the mean location of the South Pacific Anticyclone (SPAC) (identifiable in Figure 7a as the 1020 hPa contour), indicating that the SPAC has been gradually spinning up since 1979 [*Roemmich et al.*, 2007; *Marshall*, 2003]. In the 20C3m GCM ensemble the maximum subtropical SLP trend is shifted much further to the west (45°S, 160°W). Nonetheless, the overall SST-SLP association is qualitatively similar, with weak relative cooling (i.e., reduced warming) around the eastern side of the SLP anomaly and enhanced warming on the western side. A similar pattern is obtained when considering the net SLP and SST changes predicted for the next century under the SRESA2 emissions scenario (Figure 7c), in which the impacts of GHG concentrations are more readily detectable. In the A2 scenario the positive pressure anomaly in the south Pacific is wider and centered at 130°W. Once again, weak but significant temperature trend anomalies are seen on the eastern side of this feature.

[34] Although natural forcing may play some role in the trend patterns from the 20C3m scenario, the overall picture presented by Figures 7b and 7c is that at least some (i.e., 20–30%) of the SST cooling along the Chilean seaboard may be interpreted as a regional response to increased GHG concentrations and is likely governed by the southward expansion and intensification of the subtropical atmospheric gyres. The physical explanation of the apparent SLP-SST relationship is likely to reside in the enhancement of meridional winds along the coast, which in turn provoke offshore transport and coastal upwelling [e.g., *Garreaud and Falvey*, 2009]. As upwelling currents originate well below the surface [*Tomczak and Godfrey*, 1994; *Hormazabal et al.*, 2004], an enhancement of upwelling may help explain how the negative temperature trends can extend below the mixing layer. The intensification of the SPAC is also likely to

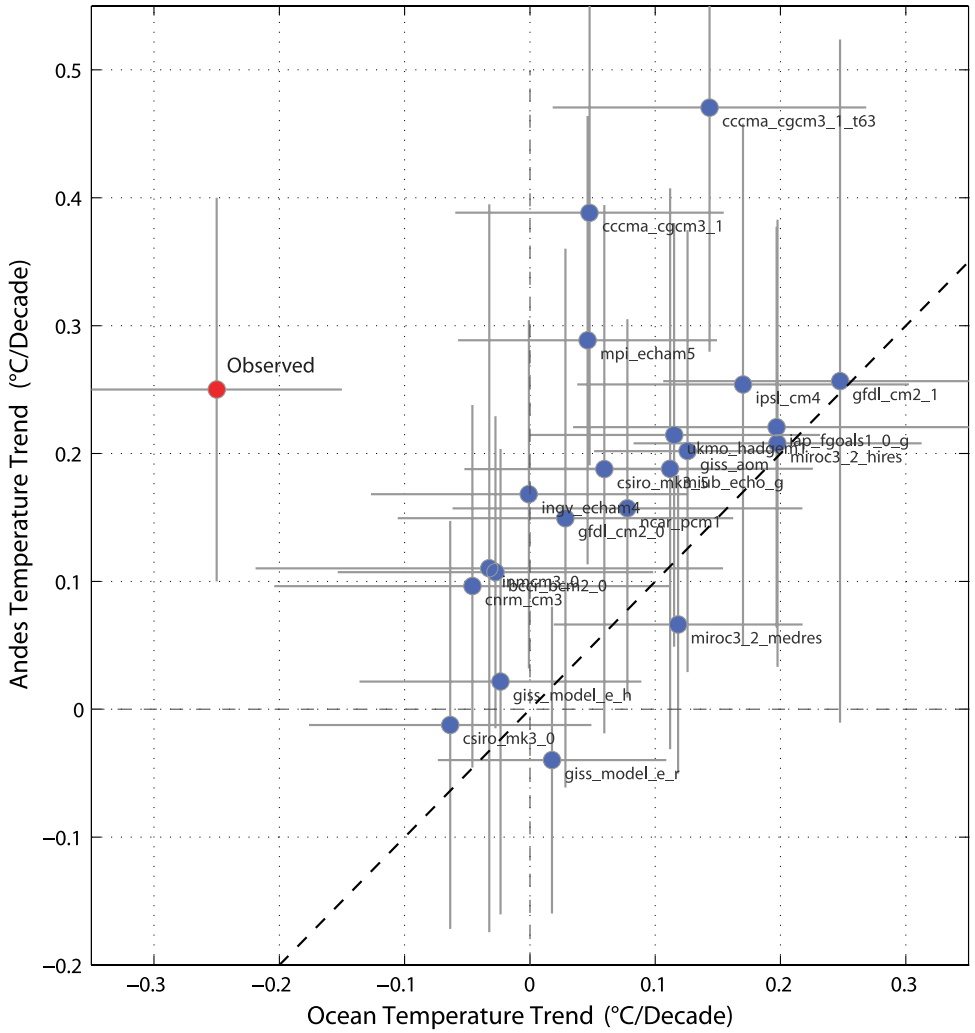

Figure 6. Scatterplot of temperature trends in central Chile (∼30°S) for the simulated period 1970–1999 (inclusive) from the CMIP-3 GCM ensemble. The horizontal axis is the SST trend at the model grid point closest to the model coastline. The vertical axis is the temperature trend above land at the highest model grid point in the Andes. The Andes are poorly resolved by all the global models and the mean model height over the land point is 1886 m (varying between about 1000 m and 3000 m for the highest and lowest resolution models, respectively), whereas the Andes actually reach well over 5000 m at this latitude. The representation of the Andes is also much wider in the global models. The mean distance between the land and sea point is 6.6° (∼700 km, and over 1000 m in some cases), when in reality it is closer to 200 km. Error bars represent the 90% confidence interval for the trends. For reference, the approximate observed value is also shown (red dot), derived qualitatively from the trends shown for the ocean and western Andes in Figure 3.

stimulate other cooling processes such as cold advection (atmospheric and oceanic), enhanced surface heat fluxes, and mixing in the upper ocean [e.g., *Kushnir et al.*, 2002; *Sen Gupta and England*, 2006]. More detailed heat budget calculations [e.g., *Huang and Liu*, 2001] will be required in order to better identify the relative importance of such processes and their relationships to the predicted circulation changes.

Figure 7. (a) Global pattern of anomalous (i.e, global mean subtracted) SST trends (°C/decade) derived from ERSST (colored squares). Thick solid (dashed) lines indicate positive (negative) SLP trends in Pa/decade derived from NCEP-NCAR Reanalysis. Thin gray lines show the climatological mean pressure field. Black crosses indicate stations in the South Pacific where long-term pressure records are available. (b) Ensemble mean of anomalous SST (colors) and SLP (solid/dashed lines) trend in the South Pacific from the CMIP-3 multimodel data set for the period 1970–1999. Gray crosses indicate regions where more than 75% of the models agree on the sign of the anomalous SST trend. The gray contours show the ensemble mean SLP field. (c) Similar to Figure 7b, but shows the differences between the periods 2071–2100 and 1970–1999 from the 20C3m and A2 emissions scenarios, respectively. The difference is expressed in the same units as Figures 7a and 7b.

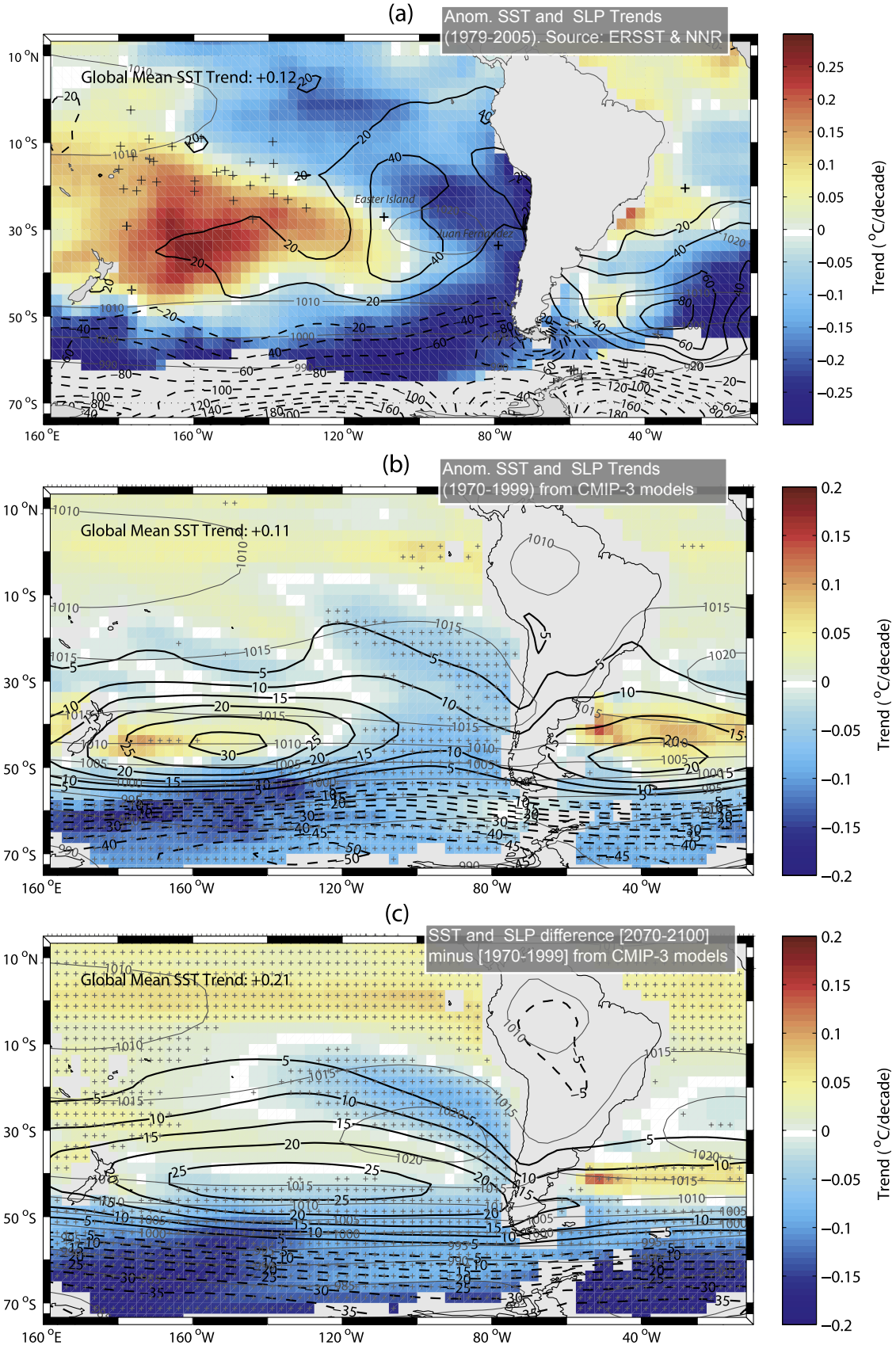
(a)
Anom. SST and SLP Trends
(1979-2005). Source: ERSST & NNR
Global Mean SST Trend: +0.12
Easter Island
Juan Fernandez
(b)
Anom. SST and SLP Trends
(1970-1999) from CMIP-3 models
Global Mean SST Trend: +0.11
(c)
SST and SLP difference [2070-2100]
minus [1970-1999] from CMIP-3 models
Global Mean SST Trend: +0.21
10 °N
10 °S
30 °S
50 °S
70 °S
160 °E
160 °W
120 °W
80 °W
40 °W
Trend (°C/decade)

Figure 7

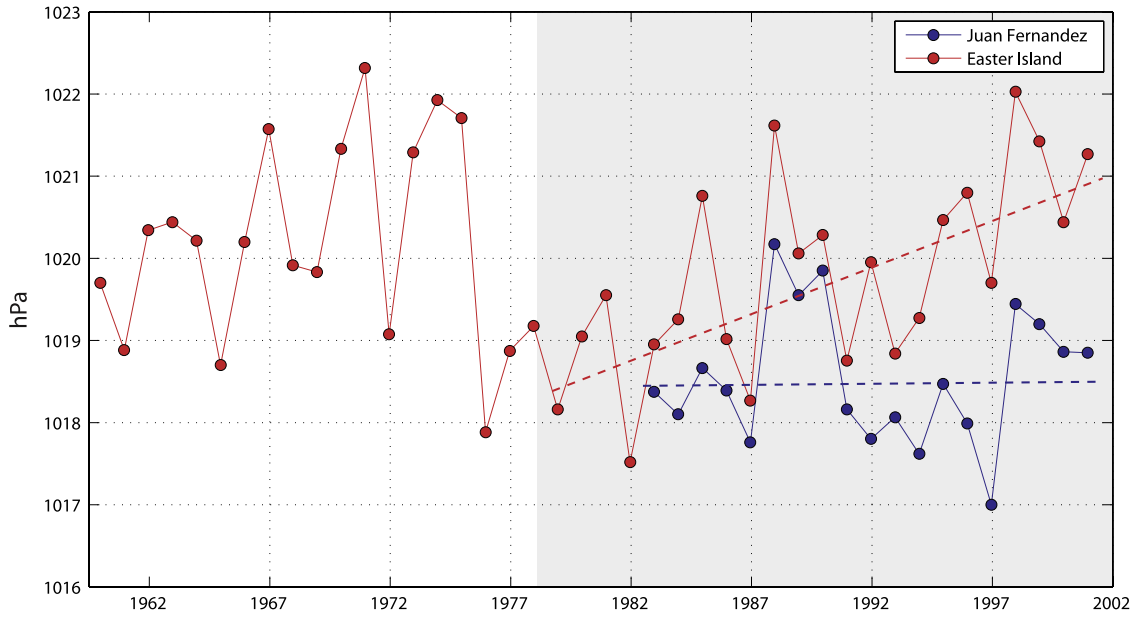

Figure 8. Time series of annual surface pressure at Easter Island and Juan Fernandez Island. The trend (dashed lines) is 110 ± 90 Pa/decade at Easter Island, and negligible at Juan Fernandez.

[35] It must be stressed that there is considerable uncertainty in the observed trends over the eastern Pacific, especially for the SLP. Over the entire South Pacific east of 120°W, there are only two long-term pressure records available (Easter and Juan Fernandez Islands, Figure 7a) and none at latitudes higher than 35°. In Figure 8 the annual SLP series (taken from the GHCN) at these two island stations are presented. After a sharp drop associated with the 1976 climate shift, the SLP at Easter Island (slightly northwest of the SPAC center) has risen by about 100 Pa/decade, twice the Reanalysis estimate at the same location. At Juan Fernandez the SLP shows no significant trend since 1983, the start of the data series (the station was moved in 1982). Thus, while the scarcity of data is clearly a major issue, both the gridded analysis and in situ records do point to a significant intensification of the SPAC, which climate models suggest may be partially related to global warming.

5. Summary and Conclusions

[36] In this study we have provided a comprehensive description of the spatial patterns of contemporary temperature trends in Chile and over the adjacent ocean for the period 1979–2006, making use of long-term records from in situ and gridded data sets. Our key observational results may be summarized as follows:

[37] 1. In central and northern Chile (17°–37°S) in situ temperature observations confirm the strong contrast between cooling off the coast (−0.20°C/decade) and warming in the central valley and western Andes (+0.25°C/decade), only 100–200 km further inland (and 500–2500 m higher). The warming rate in the western Andes is similar to that observed on the eastern (continental) side of the mountain range. In southern Chile (38°S–48°S) temperature trends over land are weak (insignificant at 90% confidence) and show no clearly identifiable spatial patterns.

[38] 2. Coastal radiosonde data (Quintero and Valparaiso) show substantial vertical structure in temperature trends, characterized by cooling near the surface and a warming maximum aloft at about 1300 m, about the same height as the top of the inversion layer. The vertical profiles compare well with land based observations at the same altitudes, thus implying that the variation between the coast and the Andes is largely a manifestation of a strong vertical stratification of trends in the atmosphere to the west of the Andes.

[39] 3. Gridded SST data (ERSST) indicate that the coastal cooling trends extend along the length of Chile's coastline. Consistent evidence of the coastal cooling is found in surface air temperature measurements, tide gauge measurements, and an alternative (HadISST) gridded product, although the HadISST trends deviate from the other data sets north of about 30°S. The coastal SST cooling forms part of a larger-scale, La Niña-like pattern that extends from the Southern Ocean to the equatorial Pacific, and this pattern is broadly consistent with the general negative trend in Pacific decadal variability (e.g., PDO) that has been observed over the same period.

[40] 4. Data from the World Ocean Database indicate that the cooling near the coast may extend below the mixed layer, to depths of at least 500 m. However, this conclusion must be treated with some caution as there is considerable uncertainty associated with the WOD trend estimates.

[41] When considering the above conclusions, it is important to bear in mind the substantial uncertainty in the trend estimates on which they are based. Owing to the relatively short time period that was examined, and the high level of interannual temperature variability, only a few of the estimated trends are nonnegligible with 90% confidence. The uncertainty range is particularly wide in northern Chile, where ENSO related interannual variability is strong. Despite these concerns, the overall consistency among different stations and measurement types suggests that the broad spatial patterns that have been identified are robust.

[42] Perhaps the most important characteristic of the trends described in this article is the strong contrast between the coastal cooling and the warming in the central valley and Andes of central and northern Chile. This result clearly demonstrates that temperature trends at low-lying stations are not representative of what is occurring in the Andes, despite the relatively short distance between the lowlands and the mountains. The Andean warming trend is well observed in central Chile but its northward extent is not well characterized by the in situ data available, although the positive trend at Calama (23°S) and the prior results of *Vuille and Bradley* [2000] provide some indication that the warming trend may extend along the length of the subtropical Andes. The positive trends in the Andes of central Chile are of considerable interest, not least because of the strong impact the warming may have on the evolution of the Andean snowpack [*Lettenmaier et al.*, 1996; *Moore and McKendry*, 1996; *Lettenmaier et al.*, 1999]. Since much of Chile's water supply is derived from meltwater, changes in seasonal snow cover and melting rates as a result of warming may have significant impacts on agriculture and hydroelectric energy generation. The altitude dependence of the warming trends may also have implications in the understanding of the causes of glacial retreat in central and northern Chile [e.g., *Vuille and Bradley*, 2000; *Bown and Rivera*, 2007]. It is noteworthy that the observed warming trend at elevated locations in central and northern Chile is consistent with the late 20th century climate change simulated by the CMIP-3 global model ensemble. The CMIP-3 models suggest that the warming trend is likely to continue, and probably intensify, throughout the 21st century as a response to increasing greenhouse gas concentrations.

[43] The interpretation of the coastal cooling pattern is somewhat more difficult. The large scale structure of the coastal cooling pattern suggests it is related to the declining PDV index from its maximum in the early 1980s [e.g., *Hartmann and Wendler*, 2005]. Although PDV is still not well understood [*Gu and Philander*, 1997; *Burgman et al.*, 2008] and may be influenced by global warming, it is widely recognized as an internally forced oscillation. Nonetheless, the fact that the ensemble mean warming is weaker along the Chilean coast than other parts of the world (except the Southern Ocean) does suggest that the predicted circulation changes act to subdue warming rates in coastal Chile, leading to temperature trend anomalies (with respect to the global mean trend) of −0.07°C/decade, about a third of the observed value. This may be a conservative estimate, as it is unlikely that the models are able to fully capture the SST response to circulation changes in the southeastern Pacific (due to their limited representation of coastal upwelling for example). Our study has provided a preliminary discussion of the changes in low-level circulation (via the SLP field) that appear to be associated with the cooling off the subtropical coast of South America. We suggest that the apparent intensification of the South Pacific Anticyclone, also a simulated consequence of global warming, is likely to play an important, perhaps driving, role. The separation of the natural and anthropogenic contributions to the long-term temperature trends in the coastal waters off Chile will require more in-depth analysis and careful consideration of the physical processes involved.

[44] **Acknowledgments.** We thank Juan Quintana and Claudia Villaroel for providing the synoptic data sets used in this study, along with Juan-Pablo Boisser and Patricio Aceituno for providing radiosonde data. We also thank the companies Aguas Andinas and Codelco for kindly providing temperature data at El Yeso and Lagunitas, respectively. The MSU/AMSU data are produced by Remote Sensing Systems and sponsored by the NOAA Climate and Global Change Program. Data are available at www.remss.com. We acknowledge the modeling groups, the Program for Climate Model Diagnosis and Intercomparison (PCMDI) and the WCRP's for their roles in making available the WCRP CMIP3 multimodel data set. Support of this data set is provided by the Office of Science, U.S. Department of Energy. This paper was greatly improved by the comments and suggestions of three anonymous reviewers. Mark Falvey and René Garreaud were both supported by the CONICYT Project ACT-19.

References

Aceituno, P. (1988), On the functioning of the Southern Oscillation in the South American sector. Part I: Surface climate, *Mon. Weather Rev.*, *116*, 505–524, doi:10.1175/1520-0493(1988)116<0505:OTFOTS>2.0.CO;2.

Bjerknes, J. (1969), Atmospheric teleconnections from the equatorial Pacific, *Mon. Weather Rev.*, *97*, 163–169, doi:10.1175/1520-0493(1969)097<0163:ATFTEP>2.3.CO;2.

Boisier, J. P., and P. Aceituno (2006), Changes in surface and upper-air temperature along the arid coast of northern Chile, paper presented at 8th International Conference on Southern Hemisphere Meteorology and Oceanography, Am. Meteorol. Soc., Foz de Iguazu, Brazil.

Bown, F., and A. Rivera (2007), Climate changes and recent glacier behavior in the Chilean Lake District, *Global Planet. Change*, *59*, 79–86, doi:10.1016/j.gloplacha.2006.11.015.

Burgman, R. J., A. C. Clement, C. M. Mitas, J. Chen, and K. Esslinger (2008), Evidence for atmospheric variability over the Pacific on decadal timescales, *Geophys. Res. Lett.*, *35*, L01704, doi:10.1029/2007GL031830.

Cai, W., and T. Cowan (2006), SAM and regional rainfall in IPCC AR4 models: Can anthropogenic forcing account for southwest Western Australian winter rainfall reduction?, *Geophys. Res. Lett.*, *33*, L24708, doi:10.1029/2006GL028037.

Cai, W., G. Shi, T. Cowan, D. Bi, and J. Ribbe (2005), The response of the Southern Annular Mode, the East Australian Current, and the southern mid-latitude ocean circulation to global warming, *Geophys. Res. Lett.*, *32*, L23706, doi:10.1029/2005GL024701.

Cane, M. A., A. C. Clement, A. Kaplan, Y. Kushnir, D. Pozdnyakov, R. Seager, S. E. Zebiak, and R. Murtugudde (1997), Twentieth-century sea surface temperature trends, *Science*, *275*, 957–960, doi:10.1126/science.275.5302.957.

Chen, J., A. D. Del Genio, B. E. Carlson, and M. Bolsilovich (2008), The spatiotemporal structure of 20th century climate variations in observations and reanalyses. Part II: Pacific pan-decadal variability, *J. Clim.*, *21*, 2634–2650, doi:10.1175/2007JCLI2012.1.

Clement, A., R. Seager, M. A. Cane, and S. E. Zebiak (1996), An ocean dynamical thermostat, *J. Clim.*, *9*, 2190–2196, doi:10.1175/1520-0442(1996)009<2190:AODT>2.0.CO;2.

Collins, M., and the CMIP Modelling Groups (2005), El Niño or La Niña like climate change?, *Clim. Dyn.*, *24*, 89–104, doi:10.1007/s00382-004-0478-x.

Cook, E. R., R. Seager, M. A. Cane, and D. W. Stahle (2007), North American drought: Reconstructions, causes, and consequences, *Earth Sci. Rev.*, *81*, 93–134, doi:10.1016/j.earscirev.2006.12.002.

de Boyer Montégut, C., G. Madec, A. S. Fischer, A. Lazar, and D. Iudicone (2004), Mixed layer depth over the global ocean: An examination of profile data and a profile-based climatology, *J. Geophys. Res.*, *109*, C12003, doi:10.1029/2004JC002378.

Garreaud, R. D., and D. S. Battisti (1999), Interannual (ENSO) and interdecadal (ENSO-like) variability in the Southern Hemisphere tropospheric circulation, *J. Clim.*, *12*, 2113–2123, doi:10.1175/1520-0442(1999)012<2113:IEAIEL>2.0.CO;2.

Garreaud, R. D., and M. Falvey (2009), The coastal winds off western subtropical South America in future climate scenarios, *Int. J. Climatol.*, doi:10.1002/joc.1716, in press.

Garreaud, R. D., M. Vuille, R. Compagnucci, and J. Marengo (2008), Present-day South American Climate, *Palaeogeogr. Palaeoclimatol. Palaeoecol.*, doi:10.1016/j.paleo.2007.10.032, in press.

Giese, B. S., S. C. Urizar, and N. S. Fukkar (2002), Southern Hemisphere origins of the 1976 climate shift, *Geophys. Res. Lett.*, *29*(2), 1014, doi:10.1029/2001GL013268.

Gille, S. T. (2008), Decadal-scale temperature trends in the Southern Hemisphere ocean, *J. Clim.*, *21*, 4749–4765.

Gillett, N. P., and D. W. J. Thompson (2003), Simulation of recent Southern Hemisphere climate change, *Science*, *302*, 273–275, doi:10.1126/science.1087440.

Gillett, N. P., T. D. Kell, and P. D. Jones (2006), Regional climate impacts of the Southern Annular Mode, *Geophys. Res. Lett.*, *33*, L23704, doi:10.1029/2006GL027721.

Gouretski, V., and K. P. Koltermann (2007), How much is the ocean really warming?, *Geophys. Res. Lett.*, *34*, L01610, doi:10.1029/2006GL027834.

Gu, D., and S. G. H. Philander (1997), Interdecadal climate fluctuations that depend on exchanges between the tropics and extratropics, *Science*, *275*, 805–807, doi:10.1126/science.275.5301.805.

Hartmann, B., and G. Wendler (2005), The significance of the 1976 Pacific climate shift in the climatology of Alaska, *J. Clim.*, *18*, 4824–4839, doi:10.1175/JCLI3532.1.

Hegerl, G. C., F. W. Zwiers, P. Braconnot, N. P. Gillett, Y. Luo, J. A. Marengo Orsini, N. Nicholls, J. E. Penner, and P. A. Stott (2007), Understanding and attributing climate change, in *Climate Change 2007*, edited by S. Solomon et al., pp. 663–745, Cambridge Univ. Press, Cambridge, U. K.

Held, I. M., and B. J. Soden (2006), Robust responses of the hydrological cycle to global warming, *J. Clim.*, *19*, 5686–5699, doi:10.1175/JCLI3990.1.

Hormazabal, S., G. Shaffer, and O. Leth (2004), Coastal transition zone off Chile, *J. Geophys. Res.*, *109*, C01021, doi:10.1029/2003JC001956.

Huang, B., and Z. Liu (2001), Temperature trend of the last 40 yr in the upper Pacific Ocean, *J. Clim.*, *14*, 3738–3750, doi:10.1175/1520-0442(2001)014<3738:TTOTLY>2.0.CO;2.

Kalnay, E., et al. (1996), The NCEP/NCAR 40-Year Reanalysis Project, *Bull. Am. Meteorol. Soc.*, *77*, 437–471, doi:10.1175/1520-0477(1996)077<0437:TNYRP>2.0.CO;2.

Klein, S., and D. Hartmann (1993), The seasonal cycle of low stratiform clouds, *J. Clim.*, *6*, 1587–1606, doi:10.1175/1520-0442(1993)006<1587:TSCOLS>2.0.CO;2.

Kushnir, Y., W. A. Robinson, I. Blade, N. M. J. Hall, S. Peng, and R. Sutton (2002), Atmospheric GCM response to extratropical SST anomalies: Synthesis and evaluation, *J. Clim.*, *15*, 2233–2256, doi:10.1175/1520-0442(2002)015<2233:AGRTES>2.0.CO;2.

Lettenmaier, D. P., G. McCabe, and E. Z. Stakiv (1996), Global climate change: effect on the hydrologic cycle, in *Handbook of Water Resources*, edited by L. W. Mays, chap. 29, pp. 3–33, McGraw-Hill, New York.

Lettenmaier, D. P., A. W. Wood, R. N. Palmer, E. F. Wood, and E. Z. Stakhiv (1999), Water resources implications of global warming: A U.S. regional perspective, *Clim. Change*, *43*, 537–579, doi:10.1023/A:1005448007910.

Levitus, S., J. Antonov, and T. Boyer (2005), Warming of the World Ocean: 1955–2003, *Geophys. Res. Lett.*, *32*, L02604, doi:10.1029/2004GL021592.

Mantua, N. J., et al. (1997), A Pacific interdecadal climate oscillation with impacts on salmon production, *Bull. Am. Meteorol. Soc.*, *78*, 1069–1079, doi:10.1175/1520-0477(1997)078<1069:APICOW>2.0.CO;2.

Marshall, G. J. (2003), Trends in the Southern Annular Mode from observations and reanalyses, *J. Clim.*, *16*, 4134–4143, doi:10.1175/1520-0442(2003)016<4134:TITSAM>2.0.CO;2.

Mears, C., A. Matthias, C. Schabel, and F. J. Wentz (2003), A reanalysis of the MSU channel 2 tropospheric temperature record, *J. Clim.*, *16*, 3650–3664, doi:10.1175/1520-0442(2003)016<3650:AROTMC>2.0.CO;2.

Miller, R. L., G. A. Schmidt, and D. T. Shindell (2006), Forced variations in the annular modes in the 20th century IPCC AR4 simulations, *J. Geophys. Res.*, *111*, D18101, doi:10.1029/2005JD006323.

Montecinos, A., and O. Pizarro (2005), Interdecadal sea surface temperature-sea level pressure coupled variability in the South Pacific Ocean, *J. Geophys. Res.*, *110*, C08005, doi:10.1029/2004JC002743.

Moore, R. D., and I. G. McKendry (1996), Spring snowpack anomaly patterns and winter climatic variability, British Columbia, Canada, *Water Resour. Res.*, *32*, 623–632, doi:10.1029/95WR03640.

Nakicenovic, N., et al. (2000), *IPCC Special Report on Emissions Scenarios*, 599 pp., Cambridge Univ. Press, New York.

Pepin, N. C., and D. J. Seidel (2005), A global comparison of surface and free-air temperatures at high elevations, *J. Geophys. Res.*, *110*, D03104, doi:10.1029/2004JD005047.

Peterson, T. C., and R. S. Vose (1997), An overview of the Global Historical Climatology Network temperature database, *Bull. Am. Meteorol. Soc.*, *78*, 2837–2849, doi:10.1175/1520-0477(1997)078<2837:AOOTGH>2.0.CO;2.

Peterson, T. C., R. Vose, R. Schmoyer, and V. Razuvaev (1998), Global Historical Climatology Network (GHCN) quality control of monthly temperature data, *Int. J. Climatol.*, *18*, 1169–1179, doi:10.1002/(SICI)1097-0088(199809)18:11<1169::AID-JOC309>3.0.CO;2-U.

Power, S., et al. (1999), Inter-decadal modulation of the impact of ENSO on Australia, *Clim. Dyn.*, *15*, 319–324, doi:10.1007/s003820050284.

Rayner, N. A., D. E. Parker, E. B. Horton, C. K. Folland, L. V. Alexander, and D. P. Rowell (2003), Global analyses of sea surface temperature, sea ice, and night marine air temperature since the late nineteenth century, *J. Geophys. Res.*, *108*(D14), 4407, doi:10.1029/2002JD002670.

Roemmich, D., et al. (2007), Decadal spin-up of the South Pacific Subtropical Gyre, *J. Phys. Oceanogr.*, *37*, 162–173, doi:10.1175/JPO3004.1.

Rosenblüth, B., H. Fuenzalida, and P. Aceituno (1997), Recent temperature variations in southern South America, *Int. J. Climatol.*, *17*, 67–85, doi:10.1002/(SICI)1097-0088(199701)17:1<67::AID-JOC120>3.0.CO;2-G.

Russell, J., K. Dixon, A. Gnanadesikan, R. J. Stouffer, and J. R. Toggweiler (2006), The Southern Hemisphere westerlies in a warming world: Propping open the door to the deep ocean, *J. Clim.*, *19*, 6382–6390, doi:10.1175/JCLI3984.1.

Rusticucci, M., and M. Barrucand (2004), Observed trends and change in temperature extremes over Argentina, *J. Clim.*, *17*, 4099–4107, doi:10.1175/1520-0442(2004)017<4099:OTACIT>2.0.CO;2.

Rutllant, J., and P. Ulriksen (1979), Boundary-layer dynamics of the extremely arid northern part of Chile, *Boundary Layer Meteorol.*, *17*, 41–55, doi:10.1007/BF00121936.

Seidel, D. J., and M. Free (2003), Comparison of lower-tropospheric temperature climatologies and trends at low and high elevation radiosonde sites, *Clim. Change*, *59*, 53–74, doi:10.1023/A:1024459610680.

Sen Gupta, A., and M. H. England (2006), Coupled ocean atmosphere ice response to variations in the Southern Annular Mode, *J. Clim.*, *19*, 4457–4486, doi:10.1175/JCLI3843.1.

Smith, T. M., and R. W. Reynolds (2004), Improved extended reconstruction of SST (1854–1997), *J. Clim.*, *17*, 2466–2477, doi:10.1175/1520-0442(2004)017<2466:IEROS>2.0.CO;2.

Tomczak, M., and J. S. Godfrey (1994), *Regional Oceanography: An Introduction*, 442 pp., Pergamon, Oxford, U. K.

Trenberth, K. E., and D. P. Stepaniak (2001), Indices of El Niño evolution, *J. Clim.*, *14*, 1697–1701, doi:10.1175/1520-0442(2001)014<1697:LIOENO>2.0.CO;2.

Trenberth, K. E., et al. (2007), Observations: Surface and atmospheric climate change, in *Climate Change 2007*, edited by S. Solomon et al., pp. 253–336, Cambridge Univ. Press, Cambridge, U. K.

Vecchi, G. A., B. J. Soden, A. T. Wittenberg, I. M. Held, A. Leetma, and M. J. Harrison (2006), Weakening of tropical Pacific atmospheric circulation due to anthropogenic forcing, *Nature*, *441*(7089), 73–76, doi:10.1038/nature04744.

Vecchi, G. A., A. Clement, and B. J. Soden (2008), Examining the tropical Pacific's response to global warming, *Eos Trans. AGU*, *89*(9), 81–83, doi:10.1029/2008EO090002.

Villarroel, C., B. Rosenbluth, and P. Aceituno (2006), Climate change along the extratropical west coast of South America (Chile): Daily max/min temperatures, paper presented at 8th International Conference on Southern Hemisphere Meteorology and Oceanography, Am. Meteorol. Soc., Foz de Iguazu, Brazil.

Vincent, L. A., et al. (2005), Observed trends in indices of daily temperature extremes in South America 1960–2000, *J. Clim.*, *18*, 5011–5023, doi:10.1175/JCLI3589.1.

Vuille, M., and R. S. Bradley (2000), Mean annual temperature trends and their vertical structure in the tropical Andes, *Geophys. Res. Lett.*, *27*(23), 3885–3888, doi:10.1029/2000GL011871.

Wallace, J. M., et al. (1999), *Reconciling Observations of Global Temperature Change*, Natl. Res. Counc., Washington, D.C.

Zhang, Y., J. M. Wallace, and D. S. Battisti (1997), ENSO-like interdecadal variability: 1900–93, *J. Clim.*, *10*, 1004–1020, doi:10.1175/1520-0442(1997)010<1004:ELIV>2.0.CO;2.

M. Falvey and R. D. Garreaud, Department of Geophysics, Universidad de Chile, Blanco Encalada 2002, Santiago, Chile. (falvey@dgf.uchile.cl)